Reaction rates for neutron capture reactions to C, N, and O isotopes to the neutron rich side of stability

H. Herndl, R. Hofinger, J. Jank, and H. Oberhummer
Institut für Kernphysik, Technische Universität Wien, Wiedner Hauptstraße 8-10, A-1040 Wien, Austria

J. Görres and M. Wiescher
Department of Physics, University of Notre Dame, Notre Dame, Indiana 46556

F.-K. Thielemann
Department für Physik und Astronomie, Universität Basel, Klingelbergstrasse 82, CH-4056 Basel, Switzerland

B. A. Brown
Department of Physics and Astronomy, Michigan State University, East Lansing, Michigan
(Received 25 June 1999; published 16 November 1999)

The reaction rates of neutron capture reactions on light nuclei are important for reliably simulating nucleosynthesis in a variety of stellar scenarios. Neutron capture reaction rates on neutron-rich C, N, and O isotopes are calculated in the framework of a hybrid compound and direct capture model. The results are tabulated and compared with the results of previous calculations as well as with experimental results.
[S0556-2813(99)04411-8]

PACS number(s): 24.50.+g, 25.40.Lw, 26.20.+f, 97.10.Cv

I. INTRODUCTION

Neutron capture processes on neutron-rich C, N, and O isotopes play an important role in astrophysical scenarios ranging from nucleosynthesis in the stellar helium and carbon burning stages to possibly inhomogeneous big bang models. To simulate the nucleosynthesis of light isotopes between carbon and neon a detailed understanding of the these neutron capture reactions is therefore essential. This paper intends to derive a consistent set of stellar neutron capture reaction rates for neutron-rich carbon, nitrogen, and oxygen isotopes, based on the latest experimental and theoretical information.

In stellar helium core burning in massive red giant stars neutrons are abundantly produced via the $^{14}\mathrm{N}(\alpha,\gamma)^{18}\mathrm{F}(\beta^{+}\nu)$ $^{18}\mathrm{O}(\alpha,\gamma)^{22}\mathrm{Ne}(\alpha,n)$ reaction sequence [1,2]. In the early helium core evolution ^{14}N and ^{18}O are initially depleted, while initiating the neutron production. The neutrons subsequently trigger the weak *s*-process component which leads to the production of intermediate mass nuclei around $A=100$. Neutrons, however, can also be captured on ^{12}C and ^{16}O which are abundantly produced in helium burning.

In the very last phase of helium core burning, the core expands and outer layers with high ^{14}N and ^{18}O abundances cause an increase in neutron production. Neutron capture on these isotopes however may act as neutron poison and may also change the light isotope abundances. This depends critically on the reaction cross section in the energy range between 25 and 200 keV.

He-shell burning in low mass asymptotic giant branch (AGB) stars has been proposed as the site for the main component of the *s* process [3–5]. Neutron production is triggered in the He-burning shell by the $^{13}\mathrm{C}(\alpha,n)$ reaction on ^{13}C being ingested by convective processes during the thermal pulses. It has been suggested that neutron induced processes on the initial and the additionally ingested carbon, nitrogen, and oxygen abundances may have considerable influence on light isotope nucleosynthesis in the thermal pulse [6,7]. Recent stellar model calculations [5] indicate that the reaction cross sections for the neutron capture processes need to be known in the energy range between 5 and 30 keV.

In the framework of inhomogeneous big bang models (IMs) high neutron flux induces primordial nucleosynthesis which bridges the mass 5 and mass 8 gap [8]. Subsequent neutron capture processes on neutron-rich carbon, nitrogen, and oxygen isotopes may bypass the long-lived ^{14}C and trigger a primordial *r* process [9–12]. The efficiency for the production of heavy elements in such a scenario depends sensitively on the respective neutron capture rates for these light isotopes. Therefore the neutron capture cross sections have to be determined over a wide energy range up to 1.0 MeV.

Over the last few years considerable effort has been made to determine the neutron capture reaction rates for the C, N, and O isotopes experimentally as well as theoretically. With the present paper we attempt to summarize the experimentally determined neutron capture rates. We present new calculations in the framework of a hybrid compound nucleus and direct capture model and compare the results with the experimental data as well as with previous calculations using the direct capture model [9] and the statistical Hauser-Feshbach model [13,14]. The same models were used to determine in addition neutron capture reaction rates on β^{-}-unstable neutron-rich C, N, and O isotopes.

In Sec. II we will present the formalism used in calculating the reaction cross sections and reaction rates. We also discuss the experimental and theoretical input parameters for the calculations of the different cross sections and reaction rates. In Sec. III the results of our calculations are compared

with previous predictions both with a direct capture and a Hauser-Feshbach model. If available we also compare our results with experimental data. Finally, in the last section the results are summarized and discussed.

II. CALCULATION OF THE REACTION RATES

The cross section for neutron capture processes is dominated by the nonresonant direct capture (DC) process and by contributions from single resonances which correspond to neutron unbound states in the compound nucleus (CN). For calculating the different reaction contributions we used a simple hybrid model: the nonresonant contributions were determined by using a direct capture model, the resonant contributions were based on determining the resonant Breit-Wigner cross section. In the case of broad resonances interference terms have to be taken into account. To determine the neutron capture cross sections on the β-unstable nuclei the necessary input parameter for the calculations (masses, Q values, spin-parity assignments of bound states and resonances, excitation energies, spectroscopic factors, density distributions, scattering data) were taken from experimental data. When no experimental data were available we used theoretical values, mainly derived from the shell model (see below).

The total reaction rate is given by

$$N_A\langle\sigma v\rangle_{\rm tot}=N_A\langle\sigma v\rangle_R+N_A\langle\sigma v\rangle_{\rm NR}+N_A\langle\sigma v\rangle_{\rm int}, \quad (1)$$

where the three terms represent the resonant contribution $N_A\langle\sigma v\rangle_R$, the nonresonant contribution $N_A\langle\sigma v\rangle_{\rm NR}$ and the interferences $N_A\langle\sigma v\rangle_{\rm int}$. Each contribution will be explained in the following sections. Another important quantity is the Maxwellian averaged cross section. For a temperature kT it is defined by

$$\frac{\langle\sigma v\rangle_{kT}}{v_T}=\frac{2}{\sqrt{(kT)^2}}\int_0^\infty E\sigma_{n,\gamma}(E)\exp\left(-\frac{E}{kT}\right)dE. \quad (2)$$

A. Resonant reaction contributions

The cross section of a single isolated resonance in neutron capture processes is well described by the Breit-Wigner formula [15,16]

$$\sigma_R(E)=\frac{\pi\hbar^2}{2\mu E}\frac{(2J+1)}{2(2j_t+1)}\frac{\Gamma_n\Gamma_\gamma}{(E_r-E)^2+(\Gamma_{\rm tot}/2)^2}, \quad (3)$$

where J and j_t are the spins of the resonance level and the target nucleus, respectively, E_r is the resonance energy. The partial widths of the entrance and exit channel are Γ_n and Γ_γ, respectively. The total width $\Gamma_{\rm tot}$ is the sum over the partial widths of all channels. The neutron partial width Γ_n can be expressed in terms of the single-particle spectroscopic factor S and the single-particle width $\Gamma_{\rm SP}$ of the resonance state [20,18]

$$\Gamma_n=C^2S\times\Gamma_{\rm SP}, \quad (4)$$

where C is the isospin Clebsch-Gordan coefficient. The single-particle width $\Gamma_{\rm SP}$ can be calculated from the scattering phase shifts of a scattering potential with the potential depth being determined by matching the resonance energy.

The gamma partial widths Γ_γ are calculated from the electromagnetic reduced transition probabilities $B(J_i\rightarrow J_f;L)$ which carry the nuclear structure information of the resonance states and the final bound states [17]. The reduced transition rates were computed within the framework of the shell model.

Most of the transitions in this work are $M1$ or $E2$ transitions. For these the relations are

$$\Gamma_{E2}[\text{eV}]=8.13\times10^{-7}E_\gamma^5[\text{MeV}]B(E2)[e^2\ \text{fm}^4] \quad (5)$$

and

$$\Gamma_{M1}[\text{eV}]=1.16\times10^{-2}E_\gamma^3[\text{MeV}]B(M1)[\mu_N^2]. \quad (6)$$

The resonant reaction rate for an isolated narrow resonance can be expressed in terms of the resonance strength $\omega\gamma$ (in units eV) [20,18]

$$N_A\langle\sigma v\rangle_r=1.54\times10^5\mu^{-3/2}T_9^{-3/2}\sum_i(\omega\gamma)_i \times\exp(-11.605E_i/T_9)\ \text{cm}^3\,\text{mole}^{-1}\,\text{s}^{-1}, \quad (7)$$

where E_i is in MeV and T_9 is the temperature in 10^9 K. The resonance strength $\omega\gamma$ for a resonance is given by

$$\omega\gamma=\frac{2J+1}{2(2j_t+1)}\frac{\Gamma_n\Gamma_\gamma}{\Gamma_{\rm tot}}. \quad (8)$$

The resonance strength has to be determined experimentally by low energy neutron capture measurements or has to be derived from the calculated partial widths.

B. Nonresonant reaction contributions

The nonresonant part of the neutron capture cross section has been calculated using the DC model described in Refs. [19,21,22]. The total cross section $\sigma_{\rm NR}$ is determined by the direct capture transitions $\sigma_i^{\rm DC}$ to all bound states with the single particle spectroscopic factors C^2S_i in the final nucleus

$$\sigma_{\rm NR}=\sum_i(C^2S)_i\sigma_i^{\rm DC}. \quad (9)$$

The DC cross sections $\sigma_i^{\rm DC}$ are determined by the overlap of the scattering wave function in the entrance channel, the bound-state wave function in the exit channel and the multipole transition operator.

In the stellar energy range considered here the nonresonant reaction cross sections are predominantly determined by s-wave and p-wave contributions. If the Q value of the neutron capture reaction is clearly higher than the neutron energy the cross section for s-wave neutron capture follows the $1/v$ law. Then the reaction rate is constant over the entire

temperature range [23]. The *s*-wave contribution to the reaction rate can then be directly determined from the thermal cross section $\sigma_{\rm th}$

$$N_A\langle\sigma v\rangle_s = N_A \times \sigma_{\rm th} v_{\rm th} \ \ {\rm cm^3\,mole^{-1}\,s^{-1}}. \tag{10}$$

The cross section for *p*-wave contributions is approximately proportional to the relative velocity v, the reaction rate is therefore proportional to the temperature [9,23,24] and can be expressed by

$$N_A\langle\sigma v\rangle_p = \frac{1.08\times 10^8}{\sqrt{\mu}} \frac{\sigma_p(E)}{\sqrt{E}} T_9 \ \ {\rm cm^3\,mole^{-1}\,s^{-1}}. \tag{11}$$

For low Q values the simple $1/v$ and v laws do not apply anymore. A significant deviation can be observed if the neutron energy is in the order of the Q value. In this case the energy dependence is given by (cf. Ref. [25] for a more detailed discussion)

$$\sigma^{E1}_{\rm DC}(s\rightarrow p) \propto \frac{1}{\sqrt{E}} \frac{(E+3Q)^2}{E+Q}, \tag{12}$$

while a transition $p\rightarrow s$ has the energy dependence

$$\sigma^{E1}_{\rm DC}(p\rightarrow s) \propto \frac{\sqrt{E}}{E+Q}. \tag{13}$$

If $E \ll Q$ the conventional energy dependence is recovered. From the above equations we obtain contributions to the reaction rate which are not constant (for *s*-wave capture) or proportional to T_9 (for *p*-wave capture) in the case of small Q values.

Several transitions considered in this work have Q values less than 1 MeV [e.g., all transitions of the reaction $^{16}{\rm C}(n,\gamma)^{17}{\rm C}$]. For these cases the neutrons are very loosely bound and the bound state wave functions reach out very far. We therefore call the deviations from the conventional energy dependence halo effects.

In the reaction $^{13}{\rm C}(n,\gamma)^{14}{\rm C}$ we also have a contribution from an incoming *d* wave. The energy dependence of *d*-wave capture is, if $E \ll Q$, proportional to $E^{3/2}$.

We now parametrize the total nonresonant reactions as a function of temperature T_9,

$$N_A\langle\sigma v\rangle_{\rm NR} = A + BT_9 - CT_9^D \ \ {\rm cm^3\,mole^{-1}\,s^{-1}}. \tag{14}$$

The first term and the second term arise from the *s*-wave and *p*-wave contribution, respectively (see above). The halo effects and the *d*-wave contributions can be fitted as CT_9^D with only a small error.

C. Interferences

If the widths of the resonances are broad an interference term has to be added. The total cross section is then given by [26]

$$\sigma(E) = \sigma_{\rm NR}(E) + \sigma_R(E) + 2[\sigma_{\rm NR}(E)\sigma_R(E)]^{1/2}\cos[\delta_R(E)]. \tag{15}$$

In this equation $\delta_R(E)$ is the resonance phase shift given by

$$\delta_R(E) = \arctan \frac{\Gamma(E)}{2(E-E_R)}. \tag{16}$$

Only the contributions with the same angular momentum of the incoming wave interfere in Eq. (15). In the capture reactions considered in this paper we find only one case where the interference between a resonance and a direct capture mechanism should be taken into account. This is the $^{13}{\rm C}(n,\gamma)^{14}{\rm C}$ reaction where the *p*-wave resonance at 143 keV interferes with the *p*-wave contribution of the direct capture. In all other cases the interference can be neglected, because either the resonance is too narrow, the resonance energy is too high or the angular momentum of the incoming partial waves of the resonant and direct capture contribution differ.

With this additional term in the cross section we have to add new terms to the reaction rate. We find that for our case of $^{13}{\rm C}(n,\gamma)^{14}{\rm C}$ the reaction rate resulting from numerical integration of Eq. (15) can be described by adding an interference term

$$N_A\langle\sigma v\rangle_{\rm int} = ET_9 + FT_9^2 \ \ {\rm cm^3\,mole^{-1}\,s^{-1}}. \tag{17}$$

D. Nuclear model input parameter

For the calculation of the single particle amplitude in both the resonant as well as nonresonant neutron capture cross sections the spectroscopic factors have to be known. These can be obtained experimentally from single particle transfer reaction studies. For example, the spectroscopic factors necessary for calculating $A(n,\gamma)B$ can be extracted from the reaction $A(d,p)B$. The γ widths can be extracted from reduced electromagnetic transition strengths. For unstable nuclei where only limited or even no experimental information is available, the spectroscopic factors and electromagnetic transition strengths can also be calculated using nuclear structure models such as the shell model (SM).

The most important ingredients in the potential model are the wave functions for the scattering and bound states in the entrance and exit channels. This is the case for the DC cross sections $\sigma_i^{\rm DC}$ in Eq. (9) as well as for the calculation of the single-particle width $\Gamma_{\rm SP}$ in Eq. (4). For the calculation of these wave functions we use real folding potentials which are given by [21,27]

$$\begin{aligned} V(R) &= \lambda V_F(R) \\ &= \lambda \int\int \rho_a(\mathbf{r}_1)\rho_A(\mathbf{r}_2) v_{\rm eff}(E,\rho_a,\rho_A,s) d\mathbf{r}_1 d\mathbf{r}_2, \end{aligned} \tag{18}$$

with λ being a potential strength parameter close to unity, and $s = |\mathbf{R}+\mathbf{r}_2-\mathbf{r}_1|$, where R is the separation of the centers of mass of the projectile and the target nucleus. The density can been derived from measured charge distributions [28] or from nuclear structure models (e.g., Hartree-Fock calculations) and the effective nucleon-nucleon interaction $v_{\rm eff}$ has been taken in the DDM3Y parametrization [27]. The imagi-

TABLE I. Comparison of the calculated neutron widths of resonance states with experimental values.

Reaction	E_x	J^π	$E_{\rm res}$ [MeV]	Γ_n (calc) [keV]	Γ_n (exp) [keV]
$^{13}C(n,\gamma)^{14}C$	8.320	2^+	0.143	3.15	3.4 ± 0.6 [a]
$^{15}N(n,\gamma)^{16}N$	3.360	1^+	0.869	21.85	15 ± 5 [b]
$^{18}O(n,\gamma)^{19}O$	4.109	$3/2^+$	0.152	0.05	<15 [c]
	4.328	$5/2^-$	0.371	6×10^{-4}	<15 [c]
	4.582	$3/2^-$	0.625	28.5	52 ± 3 [c]
	4.703	$5/2^+$	0.746	0.04	<15 [c]

[a]From Ref. [46].
[b]From Ref. [47].
[c]From Ref. [35].

nary part of the potential is very small because of the small flux into other reaction channels and can be neglected in most cases involving neutron capture by neutron-rich target nuclei.

For the calculation of the bound state wave function the parameter λ is determined from the binding energy. In the scattering channel we try to fit λ to reproduce the thermal elastic scattering cross section [29]. In general, we assume that λ is independent of both the parity and the channel spin. In a few cases, however, the incoherent scattering cross section is not negligible. Then we need to distinguish between the different possible channel spins and determine λ for each channel spin. One example for this is the neutron scattering on ^{13}C where different strength parameters are obtained due to the known incoherent scattering data.

For the calculation of the neutron widths of resonance states the parameter λ is obtained from the resonance energies. In a few cases the neutron widths calculated with Eq. (4) can be compared with experimental data. This is done in Table I. In all cases the widths agree within a factor of 2.

Detailed shell model calculations had to be performed to calculate the unknown excitation energies, spectroscopic factors and electromagnetic transition rates. The code OXBASH [30] was used for this purpose. In most cases we need to consider a combined p- and sd-shell for the neutron-rich C, N, and O isotopes. The wave functions of these isotopes are calculated with the interaction WBN from Ref. [31]. We included no more than $1p1h$ excitations from the p into the sd shell. This means that for an isotope with neutron number N the occupation number of the sd-shell is $(N-8)$ for normal parity states and $(N-7)$ for nonnormal parity states. For higher excitations the shell model dimensions become prohibitively high.

III. NEUTRON CAPTURE BY C, N, AND O ISOTOPES

Most of the neutron capture rates discussed here have been calculated previously in Ref. [9]. However, the predicted rates were handicapped by several shortcomings, mainly in the determination of the nuclear structure input parameters. First, only limited experimental and theoretical information was available about the single particle spectroscopic factors. For many unstable nuclei only rather crude estimates of the spectroscopic factors were used. Second, the electromagnetic transition strengths were not known explicitly and systematic estimates were employed. Third, for some of the unstable isotopes no experimental levels were known above the threshold. Therefore, no resonant contributions were included for these reactions.

TABLE II. Considered transitions for the direct capture reactions on C isotopes. Transitions with very small contributions are not included in the table. The spectroscopic factors are from shell model calculations unless stated otherwise. The *s*-wave transitions for the reaction $^{13}C(n,\gamma)^{14}C$ were obtained by extrapolating the thermal absorption cross section. Therefore, the spectroscopic factors for these transitions are not listed.

Reaction	Q value (MeV)	J^π	E_x (MeV)	Transition	C^2S
$^{13}C(n,\gamma)^{14}C$	8.176	0^+	0.000	$s\rightarrow1p_{1/2}$	
				$d\rightarrow1p_{1/2}$	1.734
		1^-	6.094	$p\rightarrow2s_{1/2}$	0.750 [a]
		0^+	6.589	$s\rightarrow2p_{1/2}$	
		3^-	6.728	$p\rightarrow1d_{5/2}$	0.650 [a]
		2^+	7.012	$s\rightarrow2p_{3/2}$	
		2^-	7.341	$p\rightarrow1d_{5/2}$	0.720 [a]
$^{14}C(n,\gamma)^{15}C$	1.218	$1/2^+$	0.000	$p\rightarrow2s_{1/2}$	0.980
		$5/2^+$	0.740	$p\rightarrow1d_{5/2}$	0.943
$^{15}C(n,\gamma)^{16}C$	4.251	0^+	0.000	$p\rightarrow2s_{1/2}$	0.601
		2^+	1.766	$p\rightarrow1d_{5/2}$	0.493
		0^+	3.027	$p\rightarrow2s_{1/2}$	1.344
$^{16}C(n,\gamma)^{17}C$	0.729	$3/2^+$	0.000	$p\rightarrow1d_{3/2}$	0.035
		$5/2^+$	0.032	$p\rightarrow1d_{5/2}$	0.701
		$1/2^+$	0.295	$p\rightarrow2s_{1/2}$	0.644
$^{17}C(n,\gamma)^{18}C$	4.180	0^+	0.000	$p\rightarrow1d_{3/2}$	0.103
		2^+	2.114	$p\rightarrow1d_{5/2}$	1.081
				$p\rightarrow2s_{1/2}$	0.015
		2^+	3.639	$p\rightarrow2s_{1/2}$	0.525

[a]From Ref. [46].

Using the shell model we are able to calculate spectroscopic factors, electromagnetic transition strengths, and the resonance parameters for all reactions. While it has to be admitted that the reliability of the shell model calculations decreases when we approach the dripline, we nevertheless believe that our calculations represent an important improvement compared to the previous attempts.

In the following we will discuss the neutron capture rates separately. The parameters for the direct capture are listed in Tables II, III, and IV. The parametrizations of the direct capture contribution to the reaction rate is given in Table V. The resonance parameters are listed in Tables VI, VII, and VIII.

In Figs. 1, 2, and 3 we show the cross sections determined with the help of our hybrid model for $^{13}C(n,\gamma)^{14}C$, $^{15}N(n,\gamma)^{16}N$, and $^{18}O(n,\gamma)^{19}O$ together with the experimental data from Refs. [32–35]. We also compare our reaction rates with the previously proposed ones in Figs. 4, 5, and 6. In most cases the previous theoretical rates are taken from Ref. [9], except for the reactions $^{13}C(n,\gamma)^{14}C$, $^{15}N(n,\gamma)^{16}N$, and $^{18}O(n,\gamma)^{19}O$ where we show the com-

TABLE III. Considered transitions for the direct capture reactions on *N* isotopes. Transitions with very small contributions are not included in the table. The spectroscopic factors are from shell model calculations unless stated otherwise. The *s*-wave transitions for the reaction $^{15}N(n,\gamma)^{16}N$ were obtained by extrapolating the thermal absorption cross section. These transitions are not listed in the table.

Reaction	*Q* value (MeV)	J^π	E_x (MeV)	Transition	C^2S
$^{15}N(n,\gamma)^{16}N$	2.491	2^-	0.000	$p\rightarrow 1d_{5/2}$	0.550 [a]
		0^-	0.120	$p\rightarrow 2s_{1/2}$	0.460 [a]
		3^-	0.298	$p\rightarrow 1d_{5/2}$	0.540 [a]
		1^-	0.397	$p\rightarrow 2s_{1/2}$	0.520 [a]
$^{16}N(n,\gamma)^{17}N$	5.883	$5/2^-$	1.907	$p\rightarrow 1d_{5/2}$	0.207
		$7/2^-$	3.129	$p\rightarrow 1d_{5/2}$	1.457
		$5/2^-$	4.415	$p\rightarrow 2s_{1/2}$	0.921
$^{17}N(n,\gamma)^{18}N$	2.825	2^-	0.121	$p\rightarrow 1d_{5/2}$	0.700
		3^-	0.747	$p\rightarrow 1d_{5/2}$	0.689
		1^-	1.165	$p\rightarrow 2s_{1/2}$	0.705
$^{18}N(n,\gamma)^{19}N$	5.328	$3/2^-$	1.682	$p\rightarrow 1d_{5/2}$	0.579
		$1/2^+$	2.115	$s\rightarrow 2p_{3/2}$	0.001
				$s\rightarrow 2p_{1/2}$	0.0007
		$5/2^-$	2.173	$p\rightarrow 1d_{5/2}$	0.354
		$5/2^+$	2.375	$s\rightarrow 2p_{3/2}$	0.001
		$3/2^-$	3.591	$p\rightarrow 2s_{1/2}$	0.461
		$3/2^+$	3.799	$s\rightarrow 2p_{3/2}$	0.007
				$s\rightarrow 2p_{1/2}$	0.001
		$1/2^-$	4.126	$p\rightarrow 2s_{1/2}$	0.606
		$3/2^-$	4.438	$p\rightarrow 2s_{1/2}$	0.035
		$1/2^-$	5.101	$p\rightarrow 2s_{1/2}$	0.440
		$5/2^+$	5.130	$s\rightarrow 2p_{3/2}$	0.001
		$3/2^-$	5.173	$p\rightarrow 2s_{1/2}$	0.097

[a]From Ref. [50]

parison with the experimental rates from Refs. [32–35]. In Figs. 7, 8, and 9 we compare our reaction rates with the reaction rates determined by the Hauser-Feshbach model [13].

A. $^{13}C(n,\gamma)^{14}C$

The low energy reaction cross section of $^{13}C(n,\gamma)^{14}C$ is determined by a 2^+ *p*-wave resonance at $E_n^{cm}=143$ keV which decays predominantly to the fifth excited state in ^{14}C at $E_x=7.01$ MeV (0^-) and by the nonresonant *s*-wave direct capture to the ground state and the second excited state at $E_x=6.59$ MeV (0^+). Additional *p*-wave direct capture contribution yields from the transition to the first excited state at $E_x=6.09$ MeV (1^-). Both the resonant cross section as well as the nonresonant cross sections have been measured recently [32,33]. The experimental data indicate that the total cross section is dominated by the *p*-wave resonant contribution at energies above 20 keV. The nonresonant contribution is considerably lower and agrees well with the value extrapolated by the $1/v$ law from the thermal cross section.

TABLE IV. Considered transitions for the direct capture reactions on O isotopes. Transitions with very small contributions are not included in the table. The spectroscopic factors are from shell model calculations unless stated otherwise. The *s*-wave transitions for the reaction $^{18}O(n,\gamma)^{19}O$ were obtained by extrapolating the thermal absorption cross section. Therefore, the spectroscopic factors for these transitions are not listed.

Reaction	*Q* value (MeV)	J^π	E_x (MeV)	Transition	C^2S
$^{18}O(n,\gamma)^{19}O$	3.957	$5/2^+$	0.000	$p\rightarrow 1d_{5/2}$	0.570 [a]
		$1/2^+$	1.472	$p\rightarrow 2s_{1/2}$	1.000 [a]
		$3/2^-$	3.945	$s\rightarrow 2p_{3/2}$	
$^{19}O(n,\gamma)^{20}O$	7.606	0^+	0.000	$p\rightarrow 1d_{5/2}$	3.427
		2^+	1.674	$p\rightarrow 1d_{5/2}$	0.731
				$p\rightarrow 2s_{1/2}$	0.142
		4^+	3.570	$p\rightarrow 1d_{5/2}$	1.021
		2^+	4.072	$p\rightarrow 2s_{1/2}$	0.573
		3^+	5.447	$p\rightarrow 2s_{1/2}$	0.817
$^{20}O(n,\gamma)^{21}O$	3.806	$5/2^+$	0.000	$p\rightarrow 1d_{5/2}$	0.345
		$1/2^+$	1.330	$p\rightarrow 2s_{1/2}$	0.811
$^{21}O(n,\gamma)^{22}O$	6.850	0^+	0.000	$p\rightarrow 1d_{5/2}$	5.222
		2^+	3.374	$p\rightarrow 2s_{1/2}$	0.822
		3^+	4.830	$p\rightarrow 2s_{1/2}$	0.771

[a]From Ref. [48].

To interpret the recent observational results in the framework of the model described above, we determine two potential strengths from the coherent and incoherent thermal scattering cross section. With these strengths we calculate the *s*-wave capture cross section in the channel spin formalism. The resulting theoretical thermal capture cross of 6.33 mb is larger than the experimental absorption cross section of 1.37 mb. This might partially be due to the $E1$ polarization induced by the incident neutron in the target nucleus [36]. In view of the short-range character of the nuclear forces this polarization effect is only important if the capture reaction takes place inside the nucleus. This is the case for the $s\rightarrow p$ transition in $^{13}C(n,\gamma)^{14}C$. Therefore we have extrapolated the experimental thermal cross section with an $1/v$ behavior. Other direct transitions in this reaction are incoming *p* waves where the main contributions to direct capture come from the nuclear exterior so that the polarization effect is supposed to be small.

At temperatures above 0.3 GK the reaction rate is dominated by the 143 keV resonance, at lower temperatures *p*-wave contributions determine the rate at ≈ 0.1 GK and *s*-wave contributions at temperatures $\leqslant 0.05$ GK. Since the resonance is relatively broad we cannot neglect the interference between the resonance and the *p*-wave direct capture. The interference is constructive at energies lower than the resonance energy and destructive at higher energies.

In Fig. 1 the total cross section is shown with the various contributions. At higher temperatures the *d* wave become important. The agreement with the experimental data from Refs. [32,33] is satisfactory although the energy dependence of the cross section is somewhat different. The comparison with the rate calculated on the basis of experimental data

TABLE V. Parameters for the direct capture reactions. The interference term with the parameters E and F is only used for the reaction $^{13}C(n,\gamma)^{14}C$.

	A	B	C	D	E	F
$^{13}C(n,\gamma)^{14}C$	182.310	3296.558	−5534.721	2.009	1794.927	−1103.269
$^{14}C(n,\gamma)^{15}C$		4754.286	752.370	1.630		
$^{15}C(n,\gamma)^{16}C$		2637.750	304.878	1.644		
$^{16}C(n,\gamma)^{17}C$		2861.539	1166.516	1.311		
$^{17}C(n,\gamma)^{18}C$		1334.578	337.957	1.472		
$^{15}N(n,\gamma)^{16}N$	3.18	3783.415	335.198	1.716		
$^{16}N(n,\gamma)^{17}N$		3649.913	437.549	1.633		
$^{17}N(n,\gamma)^{18}N$		3417.690	358.029	1.660		
$^{18}N(n,\gamma)^{19}N$	13.838	4051.118	966.727	1.412		
$^{18}O(n,\gamma)^{19}O$	21.357	8300.018	596.897	1.770		
$^{19}O(n,\gamma)^{20}O$		7275.368	432.266	1.747		
$^{20}O(n,\gamma)^{21}O$		6474.727	493.516	1.750		
$^{21}O(n,\gamma)^{22}O$		7327.938	543.151	1.747		

[32,33] is shown in Fig. 4. Experimental cross section data are only available in the energy range up to about 60 keV. It would be interesting to measure the cross sections at higher energies to study the interference effects with the resonance at 143 keV and compare them with our calculation. The rate is considerably lower than predicted by the Hauser-Feshbach code SMOKER as can be seen in Fig. 7. This can be explained by the low level density in the compound nucleus ^{14}C.

B. $^{14}C(n,\gamma)^{15}C$

Due to the absence of low-lying resonances the reaction rate is given by the DC contribution only. The DC transition into the ground state of ^{15}C is dominant. The high spectroscopic factor for this transition results in a clearly higher reaction rate. The reaction rate was calculated recently by Mengoni *et al.* [37]. He compares the Maxwellian averaged cross section with the measurement from Ref. [38] and another calculation from Ref. [24].

In Table IX we compare our results with these previous cross sections. Compared to both other calculations our result of 10.14 μb is slightly larger. All calculations are clearly larger than the experimental data. The reason for this discrepancy is still unknown. There are plans to remeasure the cross section.

C. $^{15}C(n,\gamma)^{16}C$

This reaction is also purely direct since there exists no resonance level near the threshold [39]. The direct capture proceeds to the 0^+ ground state, the first excited 2^+ state at 1.766 MeV and the second excited 0^+ at 3.027 MeV. Since our spectroscopic factors—especially for the transition to the second excited state—are higher than estimated in Ref. [9], the new reaction rate is larger. The new rate is also considerably lower than the predicted value by SMOKER (Fig. 7).

D. $^{16}C(n,\gamma)^{17}C$

The reaction rate is dominated by the direct transition to the second excited $1/2^+$ state at 0.295 MeV. Again the spectroscopic factor and the reaction rate are higher than estimated by Rauscher *et al.* [9] (Fig. 4) but seems to be in good agreement with the Hauser-Feshbach predictions (see Fig. 7). The contribution of the resonance at 440 keV is negligible. This resonance was recently identified experimentally by Raimann *et al.* [40]. The Maxwellian averaged cross section at 30 keV was calculated by Mengoni. In Table IX we compare our results. The cross sections differ only by about 10 %.

TABLE VI. Adopted values for the resonance parameters for capture reactions on carbon isotopes. The neutron and γ widths are calculated as explained in the text unless stated otherwise.

Reaction	E_x [MeV]	J^π	E_{res} [MeV]	Γ_n [eV]	Γ_γ [eV]	$\omega\gamma$ [eV]
$^{13}C(n,\gamma)^{14}C$	8.320	2^+	0.143	3400 [a]	0.215 [b]	0.269
$^{16}C(n,\gamma)^{17}C$	1.180	$1/2^-$	0.451	950	2.82×10^{-4}	2.82×10^{-4}
$^{17}C(n,\gamma)^{18}C$	4.864	4^+	0.684	50	6.11×10^{-4}	6.87×10^{-4}
	4.915	3^+	0.735	8450	7.37×10^{-3}	6.45×10^{-3}
	4.972	1^-	0.792	5440	5.85×10^{-2}	0.022
	4.976	2^+	0.796	8510	1.85×10^{-3}	1.16×10^{-3}

[a]From Ref. [46].
[b]From Ref. [32].

TABLE VII. Adopted values for the resonance parameters for capture reactions on nitrogen isotopes. The neutron and γ widths are calculated as explained in the text unless stated otherwise.

Reaction	E_x [MeV]	J^π	E_{res} [MeV]	Γ_n [eV]	Γ_γ [eV]	$\omega\gamma$ [eV]
^{15}N$(n,\gamma)^{16}$N	3.360	1^+	0.862	15 000 [a]	0.455	0.341
^{16}N$(n,\gamma)^{17}$N	5.904	$7/2^-$	0.021	0.032	4.80×10^{-2}	0.015
	6.121	$5/2^+$	0.238	1.2	4.80×10^{-2}	0.027
	6.325	$3/2^+$	0.442	20	5.46×10^{-2}	0.022
	6.372	$7/2^+$	0.489	20	1.52×10^{-2}	0.012
	6.373	$5/2^+$	0.490	600	0.110	0.066
	6.470	$1/2^+$	0.587	1 750	2.510	0.501
	6.685	$3/2^-$	0.802	12 500	5.660	2.263
	6.737	$7/2^+$	0.854	70	4.17×10^{-2}	0.033
	6.835	$3/2^+$	0.952	360	0.478	0.191
^{17}N$(n,\gamma)^{18}$N	2.875	3^-	0.050	1.6	9.61×10^{-3}	0.017
	2.949	2^+	0.124	1390	9.72×10^{-2}	0.121
	3.068	1^+	0.243	1060	0.209	0.157
	3.374	3^+	0.549	50	0.107	0.187
	3.437	2^-	0.612	10 180	0.517	0.646
	3.631	0^+	0.806	2350	6.26×10^{-2}	0.016
	3.644	1^-	0.819	2370	0.319	0.239
	3.722	2^+	0.897	190	4.48×10^{-2}	0.056
^{18}N$(n,\gamma)^{19}$N	5.335	$3/2^+$	0.007	7.8	0.128	0.050
	5.479	$3/2^+$	0.151	70	0.072	0.029
	5.498	$7/2^+$	0.170	40	2.40×10^{-2}	0.019
	5.634	$9/2^-$	0.306	120	5.72×10^{-4}	5.7×10^{-4}
	5.770	$5/2^+$	0.442	170	4.28×10^{-2}	0.026
	5.778	$3/2^+$	0.450	120	0.320	0.128
	5.858	$3/2^-$	0.530	8470	2.520	1.008
	5.955	$7/2^+$	0.627	180	8.26×10^{-2}	0.066
	6.006	$5/2^+$	0.678	190	4.85×10^{-2}	0.029
	6.094	$7/2^-$	0.766	9990	0.306	0.245
	6.125	$7/2^+$	0.797	950	5.08×10^{-2}	0.041
	6.128	$3/2^+$	0.800	140	1.130	0.448
	6.130	$5/2^+$	0.802	310	7.86×10^{-2}	0.047
	6.152	$1/2^+$	0.824	2090	1.100	0.220

[a]From Ref. [47].

E. ^{17}C$(n,\gamma)^{18}$C

From the shell model calculations we obtain four resonances in the energy range between $E_r=684$ keV and $E_r=796$ keV. The reaction rate is only slighty dependent on these resonances, because the resonance energies are more than 700 keV above threshold For lower temperatures the direct capture dominates. This rate has not been calculated previously, yet the calculated rate is in reasonable agreement with the prediction by the Hauser-Feshbach model. This agreement seems to be a fortuitous circumstance.

F. ^{15}N$(n,\gamma)^{16}$N

The reaction has been investigated at energies between 25 and 400 keV, recently [34]. The cross section is clearly dominated by *p*-wave transitions for energies below 500 keV. The *s*-wave contribution, which is obtained from an extrapolation of the thermal absorption cross section, is negligible at thermonuclear energies.

In Fig. 2 the cross section is compared with the measured data points from Ref. [34]. The agreement is very good. The resulting reaction rate is in good agreement with previous calculations [9]. The present calculation is also very similar to the calculations in Ref. [34]. The small difference is due to the use of a folding potential in this work.

G. ^{16}N$(n,\gamma)^{17}$N

Several unbound levels in ^{17}N are known from transfer and β-delayed neutron decay studies [41,42]. However, no spin assignment is available for the states in the stellar energy range. While the shell model predicts several levels in this energy region the available information does not allow identification of the levels with their experimental counterparts. Therefore we used the shell model energies in our

TABLE VIII. Adopted values for the resonance parameters for capture reactions on oxygen isotopes. The neutron and γ widths are calculated as explained in the text unless stated otherwise.

Reaction	E_x [MeV]	J^π	E_{res} [MeV]	Γ_n [eV]	Γ_γ [eV]	$\omega\gamma$ [eV]
$^{18}O(n,\gamma)^{19}O$	4.109	$3/2^+$	0.152	50	1.4×10^{-2}	0.028
	4.328	$5/2^-$	0.371	0.6	0.600	0.900
	4.582	$3/2^-$	0.625	52 000 [a]	1.900	3.800
	4.703	$5/2^+$	0.746	40	0.500	1.483
$^{19}O(n,\gamma)^{20}O$	7.622	3^-	0.015	11	6.52×10^{-2}	0.038
	7.622	4^+	0.015	1.1	1.11×10^{-2}	8.24×10^{-3}
	7.638	4^-	0.031	2.3	1.82×10^{-2}	0.014
	7.646	2^-	0.039	3.3	0.109	0.044
	7.739	1^-	0.132	550	12.33	3.015
	7.754	4^+	0.147	1190	0.301	0.226
	7.855	5^-	0.248	1.8	1.45×10^{-2}	0.013
	7.970	2^+	0.363	2480	4.46×10^{-2}	0.019
	8.160	3^-	0.553	2890	0.352	0.205
	8.403	1^-	0.796	9150	0.362	0.090
	8.439	2^-	0.832	2090	0.333	0.139
	8.533	3^-	0.926	8840	0.688	0.401
	8.552	2^-	0.945	1480	0.238	0.099
	8.558	3^+	0.951	20 000	0.320	0.187
$^{20}O(n,\gamma)^{21}O$	4.343	$5/2^-$	0.536	0.8	0.121	0.316
	4.765	$3/2^-$	0.958	5450	0.631	1.262
$^{21}O(n,\gamma)^{22}O$	6.863	4^+	0.014	0.7	6.83×10^{-4}	5.12×10^{-4}
	7.357	4^+	0.508	26 810	2.20×10^{-3}	1.65×10^{-3}
	7.397	2^-	0.548	780	0.014	5.83×10^{-3}
	7.472	3^-	0.623	790	0.023	0.013
	7.515	1^-	0.666	42 710	0.146	0.036

[a]From Ref. [35].

calculation for the resonant contribution. In Ref. [9] the experimental energy of the 198 keV resonance was used with a hypothetical $5/2^+$ assignment.

The difference in resonance energies in the previous and the present calculations explains the ratio of the rates. Moreover, the inclusion of the direct transition to a $5/2^-$ state at 4.415 MeV with a spectroscopic factor close to unity leads to an enhancement of the reaction rate (see Fig. 5). Yet the rate is considerably lower than the rate predicted by the Hauser-Feshbach model as shown in Fig. 8.

H. $^{17}N(n,\gamma)^{18}N$

Several bound states in ^{18}N have been identified in transfer, charge exchange, and ^{18}C β-decay studies [43]. The measurement of the β-delayed neutron decay of ^{18}C [42] yields information about some neutron unbound states, but

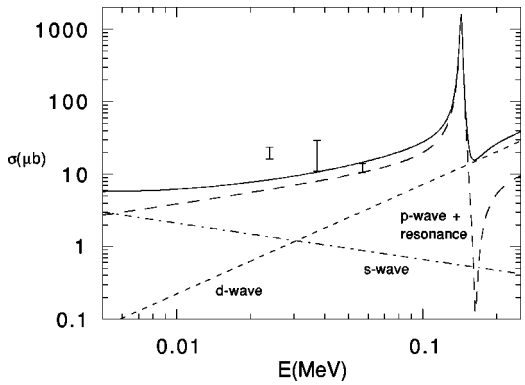

FIG. 1. Calculated cross section of the reaction $^{13}C(n,\gamma)^{14}C$ compared with experimental data from Refs. [32,33].

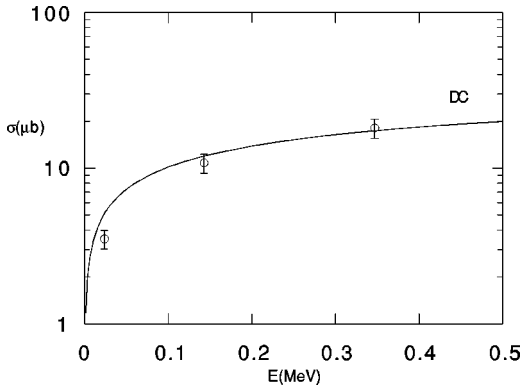

FIG. 2. Calculated cross section of the reaction $^{15}N(n,\gamma)^{16}N$ compared with experimental data from Ref. [34].

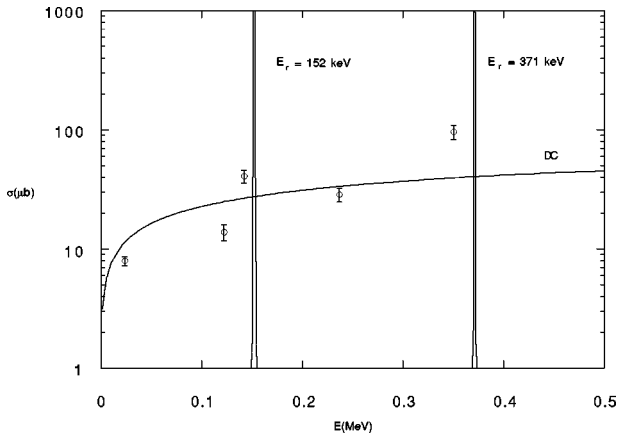

FIG. 3. Calculated cross section of the reaction $^{18}\mathrm{O}(n,\gamma)^{19}\mathrm{O}$ compared with experimental data from Ref. [35].

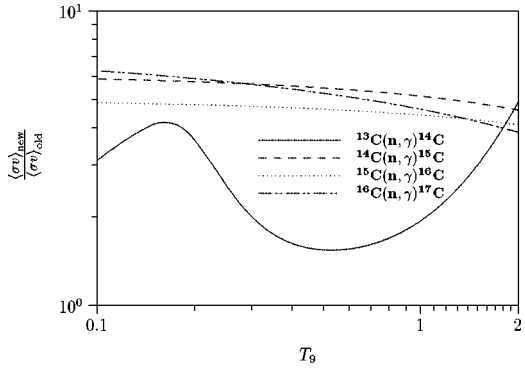

FIG. 4. Comparison of our new reaction rates for neutron capture on C isotopes with previous direct capture calculations. Shown is the ratio of the new rates to the rates published in Ref. [9] for all rates except $^{13}\mathrm{C}(n,\gamma)^{14}\mathrm{C}$ where the ratio to the rate determined from the experimental data of Refs. [32,33] is shown.

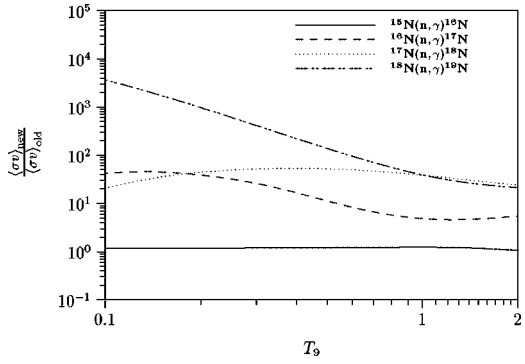

FIG. 5. Comparison of our new reaction rates for neutron capture on *N* isotopes with previous direct capture calculations. Shown is the ratio of the new rates to the rates published in Ref. [9] for all rates except $^{15}\mathrm{N}(n,\gamma)^{16}\mathrm{N}$ where the ratio to the rate determined from the experimental data of Ref. [34] is shown.

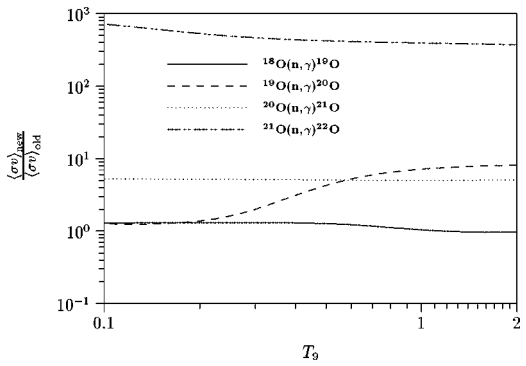

FIG. 6. Comparison of our new reaction rates for neutron capture on O isotopes with previous direct capture calculations. Shown is the ratio of the new rates to the rates published in Ref. [9] for all rates except $^{18}\mathrm{O}(n,\gamma)^{19}\mathrm{O}$ where the ratio with the rates determined from the experimental data of Ref. [35] is shown.

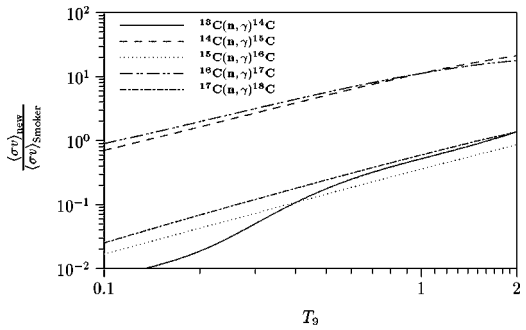

FIG. 7. Comparison of our reaction rates for neutron capture on C isotopes with Hauser-Feshbach calculations obtained with the code SMOKER.

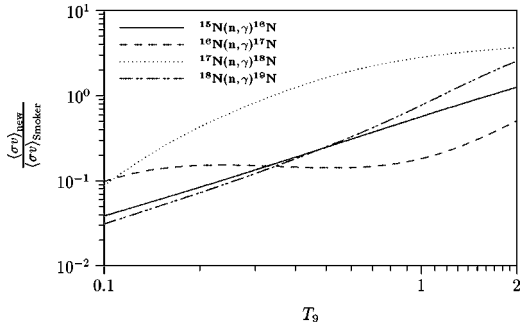

FIG. 8. Same as Fig. 7 for neutron capture of N isotopes.

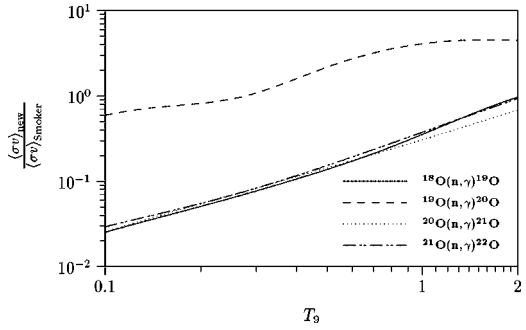

FIG. 9. Same as Fig. 7 for neutron capture of O isotopes.

the identified levels are too high in excitation energy to be of relevance for the neutron capture process discussed here. Due to the lack of experimental information about potential resonance levels its contribution was calculated on the basis of shell model predictions for level energies and single particle strengths. The strongest contribution to its direct capture components is the transition to a 1^- state at 1.165 MeV with a spectroscopic factor of 0.7. This transition was not included in the previous calculation [9]. Our rate is more than one order of magnitude larger than the previous estimate [9] but seems to agree reasonably well with the Hauser-Feshbach calculation.

I. ^{18}N$(n,\gamma)^{19}$N

Only very limited experimental information is available about the level structure of ^{19}N [43]. Multiparticle transfer studies identified some of the excited bound states and helped to determine the corresponding excitation energies. In the study of the β-delayed neutron emission of ^{19}C [44] several neutron unbound levels above 6.3 MeV were observed. No states, however, were identified near the neutron threshold of 5.32 MeV. We therefore rely in our estimate on shell model predictions only. A resonance a few keV above the threshold dominates the reaction rate for temperatures below $T_9=1$. According to the factor $\exp(-11.605E_i/T_9)$ in Eq. (7) the resonant reaction rate varies by about a factor of 2 when assuming an uncertainty of the resonance energy from 0–50 keV. According to the factor $\exp(-11.605E_i/T_9)$ in Eq. (7) the resonant reaction rate varies by about a factor of 2 at $T_9=1$ when assuming an uncertainty of the resonance energy from 0–50 keV.

In this temperature range our rate is therefore two to four orders of magnitude larger compared to Ref. [9]. For higher temperatures other resonances become important which is indicated by the agreement with the Hauser-Feshbach estimate for higher temperatures (Fig. 8).

J. ^{18}O$(n,\gamma)^{19}$O

The cross section for this reaction was recently measured over a wide energy range between 25 and 400 keV [35]. The theoretical analysis took into account possible *s*- and *p*-wave transitions to the ground state and the first excited states as well as contributions from previously observed but unpublished higher energy resonances [45]. While the present evaluation is based on the same resonance parameters, the direct capture cross section has been reevaluated to improve the extrapolation of the data over the entire energy range. The present reaction rate differs only slightly from the previous result. The *s* wave is determined by a transition to a state a few keV below the threshold. Neither the spin assignment nor the energy are known exactly. We extrapolate the experimental thermal cross section with an $1/v$ behavior to determine the *s*-wave contribution. In Fig. 3 we compare the calculated cross section with the experimental data from Ref. [35]. The data points at weighted neutron energies of 150 and 370 keV are clearly enhanced.

TABLE IX. Comparison of the Maxwellian averaged cross section $\langle\sigma v\rangle/kT$ at $kT=30$ keV with other works.

Reaction	This work	Ref. [37]	Ref. [24]	Ref. [38]
^{14}C$(n,\gamma)^{15}$C	10.14	8.3	8.4	1.87 ± 0.43
^{16}C$(n,\gamma)^{17}$C	4.71	4.3		

The calculated reaction rate agrees very well with the calculation of Ref. [35]. Again the small difference is primarily due to the use of a folding potential.

K. ^{19}O$(n,\gamma)^{20}$O

Several excited states—two of them forming a doublet at 7.622 MeV excitation energy—are known in the compound nucleus ^{20}O above the neutron threshold at 7.608 MeV [48,49]. These states could be identified with shell model levels. From the shell model we also obtain a number of additional resonance states. The previous reaction rate included only two resonances. For high temperatures our rate is therefore about one order of magnitude larger than the previous estimate (Fig. 6) but seems to be in good agreement with the Hauser-Feshbach calculation (Fig. 9).

L. ^{20}O$(n,\gamma)^{21}$O

The shell model predicts for the first excited state above the $5/2^+$ ground state of ^{21}O a spin and parity of $1/2^+$ and an excitation energy of 1.33 MeV. With a high spectroscopic factor of 0.811 the direct $p\rightarrow s$ transition to this state dominates the reaction rate. Previously only the transition to the ground state was taken into account. Therefore the new rate is higher by a factor of approximately 5. The contributions of the two resonances are small.

M. ^{21}O$(n,\gamma)^{22}$O

The new reaction rate is between two and three orders of magnitude higher. The spectroscopic factor for the transition to the ground state is 5.222, much higher than 0.2, which was estimated in Ref. [9]. Still, the transitions to two excited states are larger than the ground state transition since they are $p\rightarrow s$ transitions. Moreover, the resonance at 14 keV contributes at low temperatures.

IV. SUMMARY AND DISCUSSION

CNO isotopes can act as neutron poisons in *s*-process environments such as red giants or asymptotic giant branch

stars. They might also serve as pathways to the production of heavier nuclei in inhomogeneous big bang environments. In either case, high accuracy cross sections and reaction rates are strongly needed for relevant and precise nucleosynthesis predictions.

In the present paper we combine the latest experimental information based on cross section measurements (for stable target nuclei) and on indirect measurements of transfer, charge exchange and decay processes (for radioactive target nuclei) with theoretical direct capture and shell model calculations to derive reliable rates for neutron capture on neutron-rich C, N, and O isotopes. Thus, the reaction rates provided here contain the latest information available and should replace the corresponding rates given in previous compilations [9,10,12].

ACKNOWLEDGMENTS

This work was supported by Fonds zur Förderung der wissenschaftlichen Forschung (FWF Project No. P13246-TPH).

[1] I. Iben, Jr., Astrophys. J. **196**, 525 (1976); **196**, 549 (1976).
[2] F. Käppeler, M. Wiescher, U. Giesen, J. Görres, I. Baraffe, M. El Eid, M. Busso, C. Raitieri, R. Gallino, A. Chieffi, and M. Limongi, Astrophys. J. **437**, 396 (1994).
[3] D. E. Hollowell and I. Iben, Astrophys. J. Lett. **333**, L25 (1988).
[4] F. Käppeler, R. Gallino, M. Busso, G. Picchio, and C. Raitieri, Astrophys. J. **354**, 630 (1990).
[5] O. Straniero, R. Gallino, M. Busso, A. Chieffi, C. Raitieri, M. Salaris, and M. Limongi, Astrophys. J. Lett. **440**, L85 (1995).
[6] M. Forestini, S. Goriely, A. Jorissen, and M. Arnould, Astron. Astrophys. **261**, 157 (1992).
[7] A. Jorissen, V. V. Smith, and D. L. Lambert, Astron. Astrophys. **261**, 164 (1992).
[8] J. H. Applegate, C. J. Hogan, and R. J. Scherrer, Astrophys. J. **329**, 572 (1988).
[9] T. Rauscher, J. H. Applegate, J. J. Cowan, F.-K. Thielemann, and M. Wiescher, Astrophys. J. **429**, 499 (1994).
[10] D. Thomas, D. N. Schramm, K. A. Olive, and B. D. Fields, Astrophys. J. **406**, 569 (1993).
[11] D. Thomas, D. N. Schramm, K. A. Olive, G. J. Mathews, B. S. Meyer, and B. D. Fields, Astrophys. J. **430**, 291 (1994).
[12] M. Orito, T. Kajino, R. N. Boyd, and G. J. Mathews, Astrophys. J. **488**, 515 (1997).
[13] J. J. Cowan, F.-K. Thielemann, and J. W. Truran, Phys. Rep. **208**, 267 (1991).
[14] T. Rauscher, F.-K. Thielemann, K.-L. Kratz, Phys. Rev. C **56**, 1613 (1997).
[15] R. G. Breit and E. P. Wigner, Phys. Rev. **49**, 519 (1936).
[16] J. M. Blatt and V. F. Weisskopf, *Theoretical Nuclear Physics* (Wiley, New York, 1962).
[17] P. J. Brussaard and P. W. M. Glaudemans, *Shell Model Applications in Nuclear Spectroscopy* (North Holland, Amsterdam, 1977).
[18] H. Herndl, J. Görres, M. Wiescher, B. A. Brown, and L. van Wormer, Phys. Rev. C **52**, 1078 (1995).
[19] K. H. Kim, M. H. Park, and B. T. Kim, Phys. Rev. C **35**, 363 (1987).
[20] M. Wiescher and K.-U. Kettner, Astrophys. J. **263**, 891 (1982).
[21] H. Oberhummer and G. Staudt, in *Nuclei in the Cosmos*, edited by H. Oberhummer (Springer-Verlag, Berlin, 1991), p. 29.
[22] P. Mohr, H. Abele, R. Zwiebel, G. Staudt, H. Krauss, H. Oberhummer, A. Denker, J. W. Hammer, and G. Wolf, Phys. Rev. C **48**, 1420 (1993).
[23] W. A. Fowler, C. R. Caughlan, and B. A. Zimmerman, Annu. Rev. Astron. Astrophys. **5**, 525 (1967).
[24] M. Wiescher, J. Görres, and F.-K. Thielemann, Astrophys. J. **363**, 340 (1990).
[25] H. Oberhummer, H. Herndl, R. Hofinger, and Y. Yamamoto, *Proceedings of the Seventh Workshop in Nuclear Astrophysics*, Ringberg Castle, Bad Wiessee, edited by W. Hillebrandt and H. Müller (Max-Plank-Institut für Physik und Astrophysik, Garching, Germany, 1996), p. 46.
[26] C. Rolfs and R. E. Azuma, Nucl. Phys. **A227**, 291 (1974).
[27] A. M. Kobos, B. A. Brown, R. Lindsay, and G. R. Satchler, Nucl. Phys. **A425**, 205 (1984).
[28] H. de Vries, C. W. de Jager, and C. de Vries, At. Data Nucl. Data Tables **36**, 495 (1987).
[29] V. F. Sears, Neutron News **3**, 26 (1992).
[30] B. A. Brown, A. Etchegoyen, W. D. M. Rae, and N. S. Godwin, code OXBASH, 1984 (unpublished).
[31] E. K. Warburton and B. A. Brown, Phys. Rev. C **46**, 923 (1992).
[32] S. Raman, M. Igashira, Y. Dozono, H. Kitazawa, M. Mizumoto, and J. E. Lynn, Phys. Rev. C **41**, 458 (1990).
[33] T. Shima, F. Okazaki, T. Kikuchi, T. Kobayashi, T. Kii, T. Baba, Y. Nagai, and M. Igashira, Nucl. Phys. **A621**, 231c (1997).
[34] J. Meissner, H. Schatz, H. Herndl, M. Wiescher, H. Beer, and F. Käppeler, Phys. Rev. C **53**, 977 (1996).
[35] J. Meissner, H. Schatz, J. Görres, H. Herndl, M. Wiescher, H. Beer, and F. Käppeler, Phys. Rev. C **53**, 459 (1996).
[36] J. Zimányi, I. Halpern, and V. A. Madsen, Phys. Lett. **33B**, 205 (1970).
[37] A. Mengoni, in *Proceedings of the 1st Internet Symposium on Nuclear Data*, edited by T. Fukahori, O. Iwamoto, and T. Nakagawa, Report No. JAERI-Conf-97004, INDC-JPN-178/U (unpublished); (private communication).
[38] H. Beer, M. Wiescher, F. Käppeler, J. Görres, and P. E. Koehler, Astrophys. J. **387**, 258 (1992).
[39] R. B. Firestone, *Table of Isotopes*, 8th ed. (Wiley, New York, 1996).
[40] G. Raimann, A. Boyd, A. Ozawa, R. N. Boyd, F. R. Chloupek, M. Fujimaki, K. Kimura, T. Kobayashi, J. J. Kolata, S. Kubono, I. Tanihata, Y. Watanabe, and K. Yoshida, Phys. Rev. C **53**, 453 (1996).
[41] D. R. Tilley, H. R. Weller, and C. M. Cheves, Nucl. Phys. **A564**, 1 (1993).
[42] K. W. Scheller, J. Görres, S. Vouzoukas, M. Wiescher, B. Pfeiffer, K.-L. Kratz, D. J. Morrissey, B. M. Sherrill, M.

Steiner, M. Hellström, and J. A. Winger, Nucl. Phys. **A582**, 109 (1995).
[43] D. R. Tilley, H. R. Weller, C. M. Cheves, and R. M. Chasteler, Nucl. Phys. **A595**, 1 (1995).
[44] A. Ozawa, G. Raimann, R. N. Boyd, F. R. Chloupek, M. Fujimaki, K. Kimura, H. Kitagawa, T. Kobayashi, J. J. Kolata, S. Kubono, I. Tanihata, Y. Watanabe, and K. Yoshida, Nucl. Phys. **A592**, 244 (1995).
[45] J. Mughabghab, M. Divadeenam, and N. Nolden, *Neutron Cross Sections* (Academic Press, New York, 1981).
[46] F. Ajzenberg-Selove, Nucl. Phys. **A449**, 1 (1986).
[47] F. Ajzenberg-Selove, Nucl. Phys. **A460**, 1 (1986).
[48] F. Ajzenberg-Selove, Nucl. Phys. **A475**, 1 (1987).
[49] D. R. Tilley, C. M. Cheves, J. H. Kelley, S. Raman, and H. R. Weller, Nucl. Phys. **A636**, 249 (1998).
[50] W. Bohne, J. Bommer, H. Fuchs, K. Grabisch, H. Kluge, and G. Röschert, Nucl. Phys. **A196**, 41 (1972).